Fermionic Correlation Functions from Randomized Measurements in Programmable Atomic Quantum Devices

Piero Naldesi,[1,2] Andreas Elben,[3,4,1,2] Anna Minguzzi,[5] David Clément,[6] Peter Zoller,[1,2] and Benoît Vermersch[1,2,5]
[1]*Institute for Theoretical Physics, University of Innsbruck, Innsbruck A-6020, Austria*
[2]*Institute for Quantum Optics and Quantum Information of the Austrian Academy of Sciences, Innsbruck A-6020, Austria*
[3]*Institute for Quantum Information and Matter, Caltech, Pasadena, California 91125, USA*
[4]*Walter Burke Institute for Theoretical Physics, Caltech, Pasadena, California 91125, USA*
[5]*Univ. Grenoble Alpes, CNRS, LPMMC, 38000 Grenoble, France*
[6]*Université Paris-Saclay, Institut d'Optique Graduate School, CNRS, Laboratoire Charles Fabry, 91127, Palaiseau, France*

(Received 4 May 2022; accepted 16 March 2023; published 7 August 2023)

We provide an efficient randomized measurement protocol to estimate two- and four-point fermionic correlations in ultracold atom experiments. Our approach is based on combining random atomic beam splitter operations, which can be realized with programmable optical landscapes, with high-resolution imaging systems such as quantum gas microscopes. We illustrate our results in the context of the variational quantum eigensolver algorithm for solving quantum chemistry problems.

DOI: 10.1103/PhysRevLett.131.060601

Traditionally, quantum algorithms are run with quantum computers made of qubits. Another interesting possibility consists of using *fermionic* quantum computers with fermions as elementary constituents [1]. These devices are in particular relevant for running fermionic quantum algorithms without the technical overhead of representing fermions with qubits, e.g., via a Jordan-Wigner transformation [2]. Fermionic quantum algorithms can be used to solve numerous quantum problems. This includes quantum chemistry [3–6], the quantum simulation of fermionic quantum states relevant to high energy physics [7], and condensed matter [8]. These applications stimulate efforts to engineer fermionic quantum systems, in particular with ultracold atoms. Using programmable optical lattices or tweezer arrays [9–13], quantum gas microscopes [14–17], and time-of-flight imaging systems [18–20] one can indeed create, manipulate, and measure fermionic quantum states at high fidelity, with single-site control. However, in order to employ setups with ultracold atoms as a *fermionic quantum processor* for running fermionic quantum algorithms, there is a significant challenge to tackle: the measurement of multipoint correlations that represent the result of the computation. Here, we provide a measurement protocol based on randomized measurements [21] to access multipoint correlations, which can be implemented in existing experimental setups. For concreteness, we will illustrate our measurement protocol in the context of the variational quantum eigensolver (VQE) algorithm, where the question of high-accuracy measurements is crucial for assessing the performances of the envisioned quantum hardwares [22–25]. The protocol is, however, general and should also find applications in the context of the quantum simulation of Hubbard models with ultracold atoms [26].

VQE is a hybrid classical-quantum algorithm whose aim is to access the ground state of a quantum chemistry Hamiltonian. As we explain below, a crucial step in this algorithm is the measurement of the expectation value of the electronic Hamiltonian of a chosen molecule, which can be expressed as a linear combination of the two- and four-point fermionic correlation functions

$$C^{(1)}_{ij} = \langle c^\dagger_i c_j \rangle \quad \text{and} \quad C^{(2)}_{ijkl} = \langle c^\dagger_i c_j c^\dagger_k c_l \rangle, \tag{1}$$

where the $c^\dagger_i$ (c_i) are fermionic creation (annihilation respectively) operators. The measurement of the $C^{(1)}_{ij}$ matrix can be realized using noninteracting Hamiltonians and using a numerical inversion procedure based on a maximum likelihood algorithm [27]. Here, we will show that we can access both tensors $C^{(1)}_{ij}$, $C^{(2)}_{ijkl}$ based on simple analytical estimation formulas. Our protocol also applies to mixed states, i.e., can be used to measure correlation functions of thermal states.

Our measurement protocol takes advantage of existing high-resolution imaging systems, such as quantum gas microscopes, or single-atom-resolved detection methods after a time of flight. These methods provide snapshots of the fermionic populations in a given basis (position space or momentum space), giving access to "diagonal" correlations of the type $N_i = \langle c^\dagger_i c_i \rangle$ and $N_{ij} = \langle c^\dagger_i c_i c^\dagger_j c_j \rangle$. The system we have in mind is composed of a fermionic atomic cloud, trapped in an optical lattice. In order to access off-diagonal elements in Eq. (1), we propose to use atomic beam splitters [9]. This well-established technique effectively realizes a linear transformation of the L modes, with L being the number of lattice sites or momentum modes, of

the type $\mathbf{c}^{(U)} \equiv U \cdot \mathbf{c} = (\sum_{j=1}^{L} U_{ij} c_j)_{i=1,\ldots,L}$, where in our case U is chosen as a random unitary matrix. In the following we show that measurements performed in a fixed basis, *after* application of U, can be mapped to the desired correlations Eq. (1). This approach is adapted from the concept of randomized measurement protocols, now routinely used in qubit-type experiments [21] (see, in particular, Refs. [28,29] for accessing fermionic Hamiltonians in qubit-based quantum computers). In contrast to previous work for fermionic systems based on estimating the density matrix [30] or entanglement entropies [31,32], our protocol accesses fermionic correlations with noninteracting unitary transformations. The use of randomized measurement allows us to derive analytically efficient estimators for the desired correlations and to study numerically the required number of measurements to reach a given statistical accuracy.

The variational quantum eigensolver (VQE) with fermionic atoms.—In order to introduce our measurement protocol, we find it instructive to recall the basic steps of VQE, and to illustrate the algorithm with ultracold atoms. The setup we have in mind is depicted in Fig. 1(a). The VQE algorithm has been introduced in the context of quantum chemistry to study the electronic ground state of a molecule [22]. The electronic Hamiltonian is first cast in a second quantization form (see Supplemental Material [33]).

$$\mathcal{H}(\mathbf{R}) = \sum_{i,j=1}^{L} h_{ij}^{(1)}(\mathbf{R}) c_i^\dagger c_j + \sum_{i,j,k,l=1}^{L} h_{ijkl}^{(2)}(\mathbf{R}) c_i^\dagger c_j c_k^\dagger c_l. \quad (2)$$

The operators c_j ($c_j^\dagger$) are fermionic annihilation (creation) operators that describe electrons in a set of electronic orbitals. The coefficients $h_{ij}^{(1)}(\mathbf{R})$ and $h_{ijkl}^{(2)}(\mathbf{R})$, both explicitly depending of $\mathbf{R}$, encode the geometrical structure of the molecule, see Supplemental Material [33] for details. Since $\mathcal{H}(\mathbf{R})$ is particle number conserving, we work in a fixed sector with N spinless fermionic atoms. These N particles, placed in a one-dimensional optical lattice made of L sites, correspond to the N electrons in L electronic orbitals of the original molecule. Spinful fermions or different geometries can be also used [52–56]. The first term in $\mathcal{H}$ accounts for the single-electron problem of the molecule, i.e., the kinetic energy of the electrons and the interactions with the nuclei. The second term represents the Coulomb interactions between electrons. Because of this second term, finding the ground state of $\mathcal{H}$ is a challenging many-body problem in a Hilbert space growing exponentially with number of orbitals L.

In the VQE, one first parametrizes a set of variational wave functions $|\psi(\boldsymbol{\alpha})\rangle$, where $\boldsymbol{\alpha}$ is a vector of adjustable parameters. Note that, in order to generate the optimal wave function, it is not required to physically implement the electronic Hamiltonian $\mathcal{H}$. However, one has to measure the expectation value $\langle \mathcal{H}(\mathbf{R}) \rangle_\alpha = \langle \psi(\boldsymbol{\alpha}) | \mathcal{H}(\mathbf{R}) | \psi(\boldsymbol{\alpha}) \rangle$, which

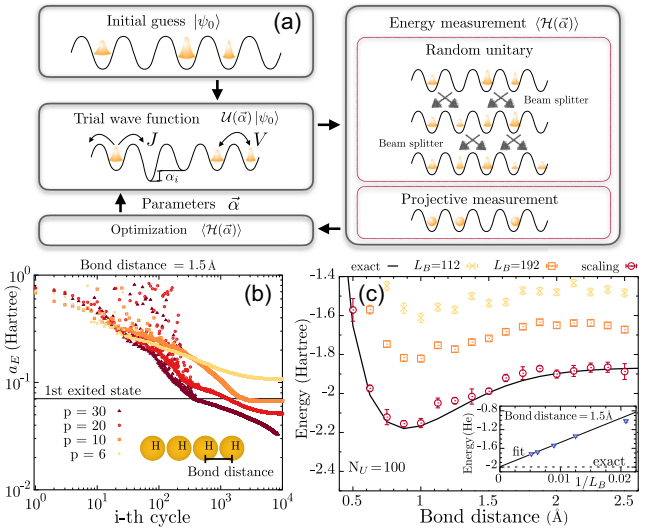

FIG. 1. Randomized measurement protocol for a fermionic variational quantum eigensolver (VQE). (a) VQE protocol with ultracold fermions in an optical lattice. First, the initial guess state $|\psi_0\rangle$ is prepared. It then enters a feedback loop composed of (i) unitary evolution $\mathcal{U}(\vec{\alpha})$, (ii) measurement of energy cost function through random unitary followed by projective measurements, and (iii) classical optimization of $\vec{\alpha}$. The loop stops when the ground state of the desired Hamiltonian has been realized in the optical lattice, within the desired error. (b) Numerical study of VQE for the H_4 molecule using the Hamiltonian Eq. (3) ($V = J = 1/T$, $N = 4$ and $L = 8$). We plot the accuracy $a_E = |E_{\mathrm{VQE}} - E|$, E being the exact ground state energy and E_{VQE} the one obtained from the VQE protocol. Larger circuit depths p, colors from light to dark are shown. The black line denotes the energy gap with the first excited state. (c) Reconstructed ground state energy as a function of the bond distance for the H_4 molecule. $N_U = 100$ random unitary transformations have been considered ($N_m = \infty$ projective measurements per unitary). Data for system sizes of $L_B = 112$, 192 the extrapolated value for $L_B \to \infty$ as well as a finite size scaling for $R = 1.5$ Å are shown.

by linearity can be achieved by accessing all correlations $C_{ij}^{(1)}$ and $C_{ijkl}^{(2)}$, see Supplemental Material [33]. The estimation $\langle \mathcal{H}(\mathbf{R}) \rangle_\alpha$, obtained on the quantum system, is then used as input for a minimization routine executed on a classical computer. This routine adjusts iteratively the parameters $\boldsymbol{\alpha}$ in order to minimize the cost function $\langle \mathcal{H}(\mathbf{R}) \rangle_\alpha$.

We show in Fig. 1(b) a numerical illustration of the VQE optimization *with ultracold atoms*. All calculations have been performed considering the standard STO-3G basis set [35]. We use standard numerical routines [37–39] to obtain the parameters $h_{ij}^{(1)}(R)$ and $h_{ijkl}^{(2)}(R)$ [57]. The code used to generate the data can be found in [58]. We study the H_4 molecule, a chain made of four hydrogen atoms, all separated by the same bond distance. In order to have significantly strong correlations between the atoms we choose a bond distance of $R = 1.5$ Å. Since we do not use any frozen-core approximation, 8 spin orbitals are considered [59]. Moreover, as the H_4 molecule has four electrons,

we consider $N = 4$ electrons in a lattice of $L = 8$ sites. The variational wave function $|\psi(\boldsymbol{\alpha})\rangle = e^{-iH_pT}\ldots e^{-iH_1T}|\psi_0\rangle$ is then generated by applying a sequence of $s = 1, \ldots, p$ time evolutions of duration T ($\hbar = 1$) to the initial state $|\psi_0\rangle$. Each of these quenches is driven by the extended Fermi-Hubbard model Hamiltonian

$$H_s = \sum_{i=1}^{L} [-J(c_{i+1}^{\dagger}c_i + \text{H.c.}) + \alpha_{i,s}n_i + Vn_i(n_{i+1})], \quad (3)$$

where the list $\boldsymbol{\alpha} = \alpha_{i,s}$ of Lp spatial and time-dependent energy potentials represent the variational parameters to be optimized. Here, V represents interactions between neighboring sites that can be obtained, for instance, using dipolar interactions with magnetic atoms [60–62]. Figure 1(b) shows the convergence of the VQE algorithm: For depths $p > 20$ and after a number of optimization cycles $> 10^2$, the algorithm reaches a state that has lower energy than the first excited state of the molecule. By increasing the number of cycles in the optimization loop, the energy keeps lowering approaching the ground state of the electronic Hamiltonian $\mathcal{H}$. The performance of the algorithm can be increased by improving the ansatz in equation Eq. (3), however, such a study is beyond the scope of our work.

The success of the VQE optimizations relies on a precise estimate of $\langle\mathcal{H}(\mathbf{R})\rangle_{\alpha}$, and therefore of the full correlators $C_{ij}^{(1)}$ and $C_{ijkl}^{(2)}$. We now present our measurement protocol giving access to such correlations. As a first illustration, Fig. 1(c) shows a simulation of the measurement of the bond dissociation curve of H_4, representing the molecular energy after the final iteration of the VQE optimization as a function of the bond distance R.

Presenting our measurement protocol.—We consider two options for implementing the measurement protocol. The first option is conceptually the simplest one but requires single-site addressing and imaging, e.g., using a quantum gas microscope. The second option is tailored instead for "time-of-flight" experiments and replaces the measurement of single site population N_i and correlations $N_{i,j}$ by the populations N_k and correlations $N_{k,k'}$ between different momentum components. For the first option, our measurement protocol begins by making the system noninteracting, e.g., by changing the dipole moment of the atoms via a change of internal levels [63,64]. This step is not required for the second option, see details below. Our measurement protocol then consists of applying successively a sequence of two-site random beam splitter operations to create a global random transformation. Two-site beam splitter operations are engineered between two adjacent lattice sites i, $i+1$, e.g., by ramping potential barriers [65] and can be realized with high fidelity in present experimental setups [9,65]. For each two-site beam splitter operation, the system then evolves according to a two-site free-fermionic Hamiltonian with the lattice operators being transformed in the Heisenberg picture as

$$\begin{pmatrix} c_i \\ c_{i+1} \end{pmatrix} \to u_i(\alpha, \phi, \psi)\begin{pmatrix} c_i \\ c_{i+1} \end{pmatrix}. \quad (4)$$

Here, $u_i(\alpha, \phi, \psi)$ is a 2×2 unitary matrix which can be parametrized by three angles $\alpha, \psi \in [0, 2\pi]$ and $\phi \in [-\pi/2, \pi/2]$ (see Supplemental Material [33] for more details). A noninteracting global unitary transformation from the circular unitary ensemble (CUE) [66] is then generated by a sequence of $L(L-1)/2$ such beam splitters $U = \prod_{j=1}^{L-1}\prod_{i=1}^{j} \mathbb{1}_i \otimes u_i(\alpha_j, \phi_{j,i}, \psi_{j,i}) \otimes \mathbb{1}_{L-i-1}$, where the angles $\alpha_j, \phi_{j,i}, \psi_{j,i}$ are sampled independently from particular distributions (see Supplemental Material [33] and the schematic Fig. 1 for more details). Note that, if using spinful fermions [48,52,55,67], one can realize the protocol by first mapping L sites to $2L$ spinless sites and then implement the beam-splitter operations as described above. Such mapping can be done using, for example, magnetic field gradients [68] and local Raman transitions.

At the end of the sequence described above, the Heisenberg operators c are transformed to $\mathbf{c}^{(U)} = U \cdot \mathbf{c}$, and a projective measurement is realized. As we have used a global noninteracting unitary U, we can easily express measurements in terms of the correlations of the system. By measuring the occupation of the lattice sites, we obtain estimates of any expectation value of the form $N_i^{(U)} = \langle c_i^{\dagger,(U)}c_i^{(U)}\rangle = \langle n_i^{(U)}\rangle$ and $N_{ij}^{(U)} = \langle n_i^{(U)}n_j^{(U)}\rangle$. This procedure (sequence of random beam splitters and projective measurement) is repeated for a number N_U of random transformations. As we show now, the statistics of these measurements yield the correlations in Eq. (1).

Extracting correlations from the measured data.—In order to extract $C_{ij}^{(1)}$ from the measured data $N_i^{(U)}$, the key idea in randomized measurements consists of using the fact that statistical correlations of random unitary transformations U can be calculated using the theory of unitary n designs [69,70]. As shown in the Supplemental Material [33], we obtain

$$C_{ij}^{(1)} = L\sum_{s_1,s_2=1}^{L}(-L)^{\delta_{s_1,s_2}-1}\overline{N_{s_2}^{(U)}U_{s_1,i}U_{s_1,j}^{*}}, \quad (5)$$

where the overline denotes the average over all different unitary transformations drawn randomly from the CUE. Here, we have used the statistical correlations between 4 matrix elements of U and used accordingly the two-design properties of the CUE. Similarly, the four-point correlation tensor $C^{(2)}$ is obtained from higher-order statistical correlations. To provide an analytical estimator, we need to consider a slight modification of our protocol: The system of L sites is embedded in a larger optical lattice of L_B sites

with $L_B > L$, these additional $L_B - L$ sites are not occupied at the beginning of the measurement sequence. The reason for this embedding is that in the limit $L_B \gg 1$, the statistical correlations of the large $L_B \times L_B$ matrices U simplify drastically: Restricting indices to a subset of values, the matrix elements U_{ij} become effectively independent Gaussian random variables, see [71] and Supplemental Material [33]. This allows us to invert the relation between the measured data and the correlations, and to write

$$C^{(2)}_{ijkl} = \sum_{\mathbf{s}=1}^{L_B} o^{(2)}_{\mathbf{s}} \overline{N^{(U)}_{s_3,s_4} U_{s_1,i} U^*_{s_1,j} U_{s_2,k} U^*_{s_2,l}} + \mathcal{O}\left(\frac{L^2}{L_B}\right) \tag{6}$$

with $\mathbf{s} = s_1, s_2, s_3, s_4$, and

$$o^{(2)}_{\mathbf{s}} = \begin{cases} (L_B-2)(L_B-3) & (s_1 = s_3) \neq (s_2 = s_4) \\ -(L_B-3) & (s_1 = s_3) \neq s_2 \neq s_4 \\ -(L_B-3) & (s_2 = s_4) \neq s_1 \neq s_3 \\ 1 & s_1 \neq s_2 \neq s_3 \neq s_4 \\ 0 & \text{otherwise.} \end{cases} \tag{7}$$

The second term in Eq. (6) represents the non-Gaussian effects of the CUE matrices, that vanishes in the limit $L_B \to \infty$. Since the embedding procedure does not affect the reconstruction of $C^{(1)}_{ij}$, both correlation matrices can be reconstructed using the same experimental data.

Protocol with a time-of-flight apparatus.—We now discuss the second option associated with time-of-flight experiments, where we propose to implement beam splitters between momentum states during a time-of-flight expansion. Here, we consider that the fermionic state is prepared using the same resources, i.e., the Fermi-Hubbard model Eq. (3). The measurement sequence is instead changed. In this second scenario, ultracold atoms are first released from the optical lattices by switching off abruptly the latter. In our regime of interest for which the lattice filling is of order unity (or less), the expansion of the gas is driven by the zero-point energy in a lattice site and it is ballistic to an excellent approximation [19,72]. After a short duration (set by the inverse of the zero-point energy in a site), the gas is diluted and exhibits the quadratic dispersion $\epsilon(k)$ of noninteracting atoms. Two-photon (Bragg) transitions then allow one to realize a beam splitter operation analogous to Eq. (4) between two momentum states [73],

$$\begin{pmatrix} \tilde{c}_k \\ \tilde{c}_{k+1} \end{pmatrix} \to u_k(\alpha, \phi, \psi) \begin{pmatrix} \tilde{c}_k \\ \tilde{c}_{k+1} \end{pmatrix}, \tag{8}$$

where $\tilde{c}_k = \sum_j c_j e^{-i2\pi kj/L_B}/\sqrt{L_B}$, $k = 0, \ldots, L-1$, are the momentum-space operators. The energy difference $\Delta\omega$ between the two Bragg beams is set to match the energy difference $\epsilon(k+1) - \epsilon(k)$ of the two coupled momentum states. Implementing many beam splitters at once is permitted by the nonlinearity of $\epsilon(k)$ and realized with multiple Bragg beams of varying energy differences $\Delta\omega$ [74]. Similarly to the first scenario, measuring the occupation of the momentum lattice sites yields expectation values of the form $\tilde{N}_k = \langle \tilde{c}^{\dagger,(U)}_k \tilde{c}^{(U)}_k \rangle = \langle \tilde{n}^{(U)}_k \rangle$, $\tilde{N}_{k,k'} = \langle \tilde{n}^{(U)}_k \tilde{n}^{(U)}_{k'} \rangle$, from which correlators of the momentum operators are estimated using Eqs. (5) and (6). Single-atom-resolved detection in time-of-flight experiments [75,76] is perfectly suited to this goal. Finally, Fourier transforms relate the correlations Eq. (1) in the position space to those measured after expansion in the momentum space.

Systematic and statistical errors.—Finally, we address quantitatively the role of systematic and statistical errors in the measurement part of the protocol. Systematic errors can arise from the miscalibration of the random unitary transformations. This effect, analyzed, for instance, for other randomized measurement protocols [77], is assessed here by adding random offsets to the three angles $\{\alpha, \phi, \psi\}$ defining each beam splitter

$$\{\alpha, \phi, \psi\} \to \{\alpha + \varepsilon\nu^\alpha, \phi + \varepsilon\nu^\phi, \psi + \varepsilon\nu^\psi\}, \tag{9}$$

where ε tunes the miscalibration and the variables $\{\nu^\alpha, \nu^\phi, \nu^\psi\}$ are picked uniformly from the interval $[-1, 1]$. A numerical study is shown in Fig. 2(a) for various values of miscalibration noise ε. The accuracy in the energy estimation is defined as $a_\varepsilon = |E_\varepsilon - E|$, with E and E_ε being, respectively, the exact energy and the one affected by miscalibration. At large values of ε, the error is maximal at large L_B. This is because the number of beam splitter operations increases with L_B, leading to the propagation of miscalibration errors. Instead, at small ε, we observe the influence of another source of systematic errors, which is

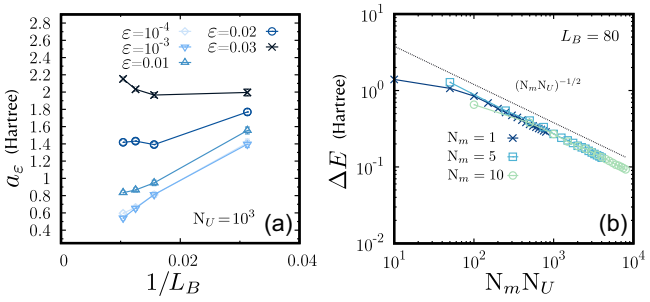

FIG. 2. Analysis of systematic and statistical errors. We study the H_4 molecule with bond distance of 1.5 Å. Here we assume that the exact GS has been prepared in the system. (a) Reconstruction error a_ε due to unitary miscalibration as a function of L_B^{-1} for increasing miscalibration strength ε (see text), colors from light to dark. Here, we consider $N_m = \infty$ and $N_U = 10^3$. (b) Scaling of statistical error ΔE as a function of the measurement budget $N_m N_U$. Here, we assume perfect beam splitters, i.e., $\varepsilon = 0$.

the error in $O(1/L_B)$ appearing in the estimation of the four-point correlations $C^{(2)}_{ijkl}$; cf. Eq. (6), see also additional numerical calculations in Supplemental Material [33]. This effect, responsible for the offset between the reconstructed and exact result, can be reduced by using a linear extrapolation for different values of $1/L_B \to 0$, as shown in Fig. 1(c). Finally, statistical errors arise from two contributions: (i) the finite number of random unitary transformations N_U used to estimate the ensemble average in Eqs. (5) and (6), (ii) the finite number of projective measurement N_m used to obtain for a given unitary U, the expectation values $N^{(U)}_{s_1}$, and $N^{(U)}_{s_1,s_2}$. In our protocol, the estimation of the ground state energy is obtained by averaging the results obtained from N_U independently sampled unitary transformations. Thus, we quantify statistical errors in terms of the standard deviation on the mean $\Delta E = \delta E/\sqrt{N_U}$, with δE being the standard deviation associated with estimates built from a single random unitary $N_U = 1$. As shown in the Supplemental Material [33] for the extreme case $N_M = 1$, the required values of N_U to estimate $C^{(1)}$ and $C^{(2)}$ scale as L^2 (L_B^2, respectively). This implies, in particular, that the measurement budget $N_m N_U$ to estimate E scales polynomially in the system size. As an illustration, we represent ΔE versus $N_m N_U$ in Fig. 2(b) for $L_B = 80$ and different values of N_m, which also shows an approximate $1/\sqrt{N_m N_U}$ dependence. These results show that fermionic correlations can be efficiently estimated accurately using our protocol.

Conclusion.—Our fermionic measurement protocol provides access to two- and four-point correlation functions in ultracold atom experiments and sets the stage to run fermionic quantum algorithms. Our work also points to several interesting research directions. We can, in particular, extend our protocol to continuous variable systems such as degenerate Fermi gases [78] to detect off-diagonal long-range order and bosonic systems [79] where emergent field theories can be explored. In this context, our protocol could also be exploited to estimate entanglement based on Gaussian entropies [80].

We thank A. Rath, R. V. Bijnen, J. Carrasco, and C. Kokail for valuable discussions. Work in Innsbruck has been supported by the European Union's Horizon 2020 research and innovation programme under Grant Agreement No. 817482 (Pasquans), by the Simons Collaboration on Ultra-Quantum Matter, which is a grant from the Simons Foundation (651440, P. Z.), and by LASCEM via AFOSR No. 64896-PH-QC. A. E. acknowledges funding by the German National Academy of Sciences Leopoldina under the Grant No. LPDS 2021-02 and by the Walter Burke Institute for Theoretical Physics at Caltech. B. V. and A. M. acknowledge funding from the French National Research Agency (ANR-20-CE47-0005, JCJC project QRand). P. N. and B. V. acknowledge funding from the Austrian Science Foundation (FWF, P 32597 N). B. V. and D. C. acknowledge funding from the France 2030 programs of the French National Research Agency [BV: EPIQ (ANR-22-PETQ-0007), and DC/BV:QUBITAF (ANR-22-PETQ-0004)]. D. C. acknowledges support from the Agence Nationale pour la Recherche (Grant No. ANR-17-CE30-0020-01) and the "Fondation d'entreprise iXcore pour la recherche."

Notes added.—Recently, a work was posted in Ref. [81] extending our findings to the measurement of arbitrary fermionic k-reduced density matrices.

[1] S. B. Bravyi and A. Y. Kitaev, Ann. Phys. (Amsterdam) **298**, 210 (2002).
[2] P. Jordan and E. Wigner, Z. Phys. **47**, 631 (1928).
[3] Y. Cao, J. Romero, J. P. Olson, M. Degroote, P. D. Johnson, M. Kieferová, I. D. Kivlichan, T. Menke, B. Peropadre, N. P. D. Sawaya *et al.*, Chem. Rev. **119**, 10856 (2019).
[4] B. Bauer, S. Bravyi, M. Motta, and G. K.-L. Chan, Chem. Rev. **120**, 12685 (2020).
[5] S. McArdle, S. Endo, A. Aspuru-Guzik, S. C. Benjamin, and X. Yuan, Rev. Mod. Phys. **92**, 015003 (2020).
[6] J. Argüello-Luengo, A. González-Tudela, T. Shi, P. Zoller, and J. I. Cirac, Nature (London) **574**, 215 (2019).
[7] M. C. Bañuls, R. Blatt, J. Catani, A. Celi, J. I. Cirac, M. Dalmonte, L. Fallani, K. Jansen, M. Lewenstein, S. Montangero *et al.*, Eur. Phys. J. D **74**, 165 (2020).
[8] A. Auerbach, *Interacting Electrons and Quantum Magnetism* (Springer Science & Business Media, New York, 2012).
[9] S. Murmann, A. Bergschneider, V. M. Klinkhamer, G. Zürn, T. Lompe, and S. Jochim, Phys. Rev. Lett. **114**, 080402 (2015).
[10] A. M. Kaufman, B. J. Lester, M. Foss-Feig, M. L. Wall, A. M. Rey, and C. A. Regal, Nature (London) **527**, 208 (2015).
[11] D. Bluvstein, H. Levine, G. Semeghini, T. T. Wang, S. Ebadi, M. Kalinowski, A. Keesling, N. Maskara, H. Pichler, M. Greiner *et al.*, Nature (London) **604**, 451 (2022).
[12] A. W. Young, W. J. Eckner, N. Schine, A. M. Childs, and A. M. Kaufman, Science **377**, 885 (2022).
[13] Z. Z. Yan, B. M. Spar, M. L. Prichard, S. Chi, H.-T. Wei, E. Ibarra-García-Padilla, K. R. A. Hazzard, and W. S. Bakr, Phys. Rev. Lett. **129**, 123201 (2022).
[14] W. S. Bakr, J. I. Gillen, A. Peng, S. Fölling, and M. Greiner, Nature (London) **462**, 74 (2009).
[15] J. F. Sherson, C. Weitenberg, M. Endres, M. Cheneau, I. Bloch, and S. Kuhr, Nature (London) **467**, 68 (2010).
[16] C. Weitenberg, M. Endres, J. F. Sherson, M. Cheneau, P. Schauß, T. Fukuhara, I. Bloch, and S. Kuhr, Nature (London) **471**, 319 (2011).
[17] C. Gross and W. S. Bakr, Nat. Phys. **17**, 1316 (2021).
[18] F. Gerbier, S. Trotzky, S. Fölling, U. Schnorrberger, J. D. Thompson, A. Widera, I. Bloch, L. Pollet, M. Troyer,

B. Capogrosso-Sansone *et al.*, Phys. Rev. Lett. **101**, 155303 (2008).
[19] H. Cayla, C. Carcy, Q. Bouton, R. Chang, G. Carleo, M. Mancini, and D. Clément, Phys. Rev. A **97**, 061609(R) (2018).
[20] P. M. Preiss, J. H. Becher, R. Klemt, V. Klinkhamer, A. Bergschneider, N. Defenu, and S. Jochim, Phys. Rev. Lett. **122**, 143602 (2019).
[21] A. Elben, S. T. Flammia, H.-Y. Huang, R. Kueng, J. Preskill, B. Vermersch, and P. Zoller, Nat. Rev. Phys. **5**, 9 (2023).
[22] A. Peruzzo, J. McClean, P. Shadbolt, M.-H. Yung, X.-Q. Zhou, P. J. Love, A. Aspuru-Guzik, and J. L. O'Brien, Nat. Commun. **5**, 4213 (2014).
[23] A. Kandala, A. Mezzacapo, K. Temme, M. Takita, M. Brink, J. M. Chow, and J. M. Gambetta, Nature (London) **549**, 242 (2017).
[24] C. Hempel, C. Maier, J. Romero, J. McClean, T. Monz, H. Shen, P. Jurcevic, B. P. Lanyon, P. Love, R. Babbush *et al.*, Phys. Rev. X **8**, 031022 (2018).
[25] F. Arute, K. Arya, R. Babbush, D. Bacon, J. C. Bardin, R. Barends, S. Boixo, M. Broughton *et al.* (Google AI QUANTUM Collaboration), Science **369**, 1084 (2020).
[26] C. Gross and I. Bloch, Science **357**, 995 (2017).
[27] M. Gluza and J. Eisert, Phys. Rev. Lett. **127**, 090503 (2021).
[28] A. Zhao, N. C. Rubin, and A. Miyake, Phys. Rev. Lett. **127**, 110504 (2021).
[29] K. Wan, W. J. Huggins, J. Lee, and R. Babbush, arXiv: 2207.13723.
[30] M. Ohliger, V. Nesme, and J. Eisert, New J. Phys. **15**, 015024 (2013).
[31] A. Elben, B. Vermersch, M. Dalmonte, J. I. Cirac, and P. Zoller, Phys. Rev. Lett. **120**, 050406 (2018).
[32] B. Vermersch, A. Elben, M. Dalmonte, J. I. Cirac, and P. Zoller, Phys. Rev. A **97**, 023604 (2018).
[33] See Supplemental Material at http://link.aps.org/supplemental/10.1103/PhysRevLett.131.060601, for further details on the derivation of electronic Hamiltonian, decomposition of CUE matrices, derivation of equations (5) and (6) of the main text, analytical study of statistical errors, and a study of systematic errors, which includes Refs. [3,17,22,34–51].
[34] J. Tilly, H. Chen, S. Cao, D. Picozzi, K. Setia, Y. Li, E. Grant, L. Wossnig, I. Rungger, G. H. Booth, and J. Tennyson, Phys. Rep. **986**, 1 (2022).
[35] T. Helgaker, P. Jørgensen, and J. Olsen, *Molecular Electronic-Structure Theory* (John Wiley & Sons, Ltd, New York, 2000), Chap. 6–8, pp. 201–335.
[36] J. R. McClean, K. J. Sung, I. D. Kivlichan, Y. Cao, C. Dai, E. Schuyler Fried, C. Gidney, B. Gimby, P. Gokhale, T. Häner *et al.*, arXiv:1710.07629.
[37] Q. Sun, J. Comput. Chem. **36**, 1664 (2015).
[38] Q. Sun, T. C. Berkelbach, N. S. Blunt, G. H. Booth, S. Guo, Z. Li, J. Liu, J. D. McClain, and E. R. Sayfutyarova, S. Sharma *et al.*, WIREs Comput. Mol. Sci. **8**, e1340 (2018).
[39] Q. Sun, X. Zhang, S. Banerjee, P. Bao, M. Barbry, N. S. Blunt, N. A. Bogdanov, G. H. Booth, J. Chen, Z.-H. Cui *et al.*, J. Chem. Phys. **153**, 024109 (2020).
[40] A. Hurwitz, Nachr. Ges. Wiss. Göttingen 71 (1897), https://eudml.org/doc/58378.
[41] P. Diaconis and P. J. Forrester, Random Matrices Theory Appl. **06**, 1730001 (2017).
[42] B. Collins, Int. Math. Res. Not. **2003**, 953 (2003).
[43] B. Collins and I. Nechita, Commun. Math. Phys. **297**, 345 (2010).
[44] A. Elben, B. Vermersch, C. F. Roos, and P. Zoller, Phys. Rev. A **99**, 052323 (2019).
[45] D. A. Roberts and B. Yoshida, J. High Energy Phys. 04 (2017) 121.
[46] C. G. Bowsher and P. S. Swain, Proc. Natl. Acad. Sci. U.S.A. **109**, E1320 (2012).
[47] H.-Y. Huang, R. Kueng, and J. Preskill, Nat. Phys. **16**, 1050 (2020).
[48] A. Mazurenko, C. S. Chiu, G. Ji, M. F. Parsons, M. Kanász-Nagy, R. Schmidt, F. Grusdt, E. Demler, D. Greif, and M. Greiner, Nature (London) **545**, 462 (2017).
[49] A. Rath, C. Branciard, A. Minguzzi, and B. Vermersch, Phys. Rev. Lett. **127**, 260501 (2021).
[50] A. Rath, R. van Bijnen, A. Elben, P. Zoller, and B. Vermersch, Phys. Rev. Lett. **127**, 200503 (2021).
[51] G. Hercé, J.-P. Bureik, A. Ténart, A. Aspect, A. Dareau, and D. Clément, Phys. Rev. Res. **5**, L012037 (2023).
[52] O. Mandel, M. Greiner, A. Widera, T. Rom, T. W. Hänsch, and I. Bloch, Nature (London) **425**, 937 (2003).
[53] O. Mandel, M. Greiner, A. Widera, T. Rom, T. W. Hänsch, and I. Bloch, Phys. Rev. Lett. **91**, 010407 (2003).
[54] M. Karski, L. Förster, J.-M. Choi, A. Steffen, W. Alt, D. Meschede, and A. Widera, Science **325**, 174 (2009).
[55] A. J. Daley, M. M. Boyd, J. Ye, and P. Zoller, Phys. Rev. Lett. **101**, 170504 (2008).
[56] A. J. Daley, J. Ye, and P. Zoller, Eur. Phys. J. D **65**, 207 (2011).
[57] J. R. McClean, K. J. Sung, I. D. Kivlichan, Y. Cao, C. Dai, E. Schuyler Fried, C. Gidney, B. Gimby, P. Gokhale, T. Häner *et al.*, Quantum Sci. Technol. **5**, 034014 (2020).
[58] P. Naldesi, Randomized measurments for fermionic correlation and quantum chemistry, https://github.com/PNaldesi/Randomized_Measurements (2022).
[59] H. L. Tang, V. O. Shkolnikov, G. S. Barron, H. R. Grimsley, N. J. Mayhall, E. Barnes, and S. E. Economou, PRX Quantum **2**, 020310 (2021).
[60] K.-K. Ni, S. Ospelkaus, D. Wang, G. Quéméner, B. Neyenhuis, M. H. G. de Miranda, J. L. Bohn, J. Ye, and D. S. Jin, Nature (London) **464**, 1324 (2010).
[61] S. Baier, M. J. Mark, D. Petter, K. Aikawa, L. Chomaz, Z. Cai, M. Baranov, P. Zoller, and F. Ferlaino, Science **352**, 201 (2016).
[62] L. Chomaz, I. Ferrier-Barbut, F. Ferlaino, B. Laburthe-Tolra, B. L. Lev, and T. Pfau, Rep. Prog. Phys. **86**, 026401 (2023).
[63] R. Lopes, C. Eigen, N. Navon, D. Clément, R. P. Smith, and Z. Hadzibabic, Phys. Rev. Lett. **119**, 190404 (2017).
[64] J. T. Stewart, J. P. Gaebler, T. E. Drake, and D. S. Jin, Phys. Rev. Lett. **104**, 235301 (2010).
[65] R. Islam, R. Ma, P. M. Preiss, M. Eric Tai, A. Lukin, M. Rispoli, and M. Greiner, Nature (London) **528**, 77 (2015).
[66] F. Mezzadri, arXiv:math-ph/0609050.
[67] D. Jaksch, H.-J. Briegel, J. I. Cirac, C. W. Gardiner, and P. Zoller, Phys. Rev. Lett. **82**, 1975 (1999).

[68] M. Boll, T. A. Hilker, G. Salomon, A. Omran, J. Nespolo, L. Pollet, I. Bloch, and C. Gross, Science **353**, 1257 (2016).
[69] D. Gross, K. Audenaert, and J. Eisert, J. Math. Phys. (N.Y.) **48**, 052104 (2007).
[70] C. Dankert, R. Cleve, J. Emerson, and E. Livine, Phys. Rev. A **80**, 012304 (2009).
[71] S. J. van Enk and C. W. J. Beenakker, Phys. Rev. Lett. **108**, 110503 (2012).
[72] A. Tenart, C. Carcy, H. Cayla, T. Bourdel, M. Mancini, and D. Clément, Phys. Rev. Res. **2**, 013017 (2020).
[73] R. Lopes, A. Imanaliev, A. Aspect, M. Cheneau, D. Boiron, and C. I. Westbrook, Nature (London) **520**, 66 (2015).
[74] B. Gadway, Phys. Rev. A **92**, 043606 (2015).
[75] T. Jeltes, J. M. McNamara, W. Hogervorst, W. Vassen, V. Krachmalnicoff, M. Schellekens, A. Perrin, H. Chang, D. Boiron, A. Aspect, and C. I. Westbrook, Nature (London) **445**, 402 (2007).
[76] A. Bergschneider, V. M. Klinkhamer, J. H. Becher, R. Klemt, G. Zürn, P. M. Preiss, and S. Jochim, Phys. Rev. A **97**, 063613 (2018).
[77] A. Elben, B. Vermersch, R. van Bijnen, C. Kokail, T. Brydges, C. Maier, M. K. Joshi, R. Blatt, C. F. Roos, and P. Zoller, Phys. Rev. Lett. **124**, 010504 (2020).
[78] M. Holten, L. Bayha, K. Subramanian, S. Brandstetter, C. Heintze, P. Lunt, P. M. Preiss, and S. Jochim, Nature (London) **606**, 287 (2022).
[79] M. Tajik, I. Kukuljan, S. Sotiriadis, B. Rauer, T. Schweigler, F. Cataldini, J. Sabino, F. Møller, P. Schüttelkopf, S.-C. Ji *et al.*, arXiv:2206.10563.
[80] J. Eisert and M. M. Wolf, arXiv:quant-ph/0505151.
[81] G. H. Low, arXiv:2208.08964.